Eliminating the "Hook" in Precipitation–Temperature Scaling

JOHAN B. VISSER,[a] CONRAD WASKO,[b] ASHISH SHARMA,[a] AND RORY NATHAN[b]

[a] *School of Civil and Environmental Engineering, University of New South Wales, Sydney, New South Wales, Australia*
[b] *Department of Infrastructure Engineering, University of Melbourne, Parkville, Victoria, Australia*

(Manuscript received 13 April 2021, in final form 2 September 2021)

ABSTRACT: Observational studies of extreme daily and subdaily precipitation–temperature sensitivities (apparent scaling) aim to provide evidence and improved understanding of how extreme precipitation will respond to a warming climate. However, interpretation of apparent scaling results is hindered by large variations in derived scaling rates and divergence from theoretical and modeled projections of systematic increases in extreme precipitation intensities (climate scaling). In warmer climatic regions, rainfall intensity has been reported to increase with temperature to a maximum before decreasing, creating a second-order discontinuity or "hook"-like structure. Here we investigate spatial and temporal discrepancies in apparent scaling results by isolating rainfall events and conditioning event precipitation on duration. We find that previously reported negative apparent scaling at higher temperatures that creates the hook structure is the result of a decrease in the duration of the precipitation event, and not a decrease in the precipitation rate. We introduce standardized pooling using long records of Australian station data across climate zones to show average precipitation intensities and 1-h peak precipitation intensities increase with temperature across all event durations and locations investigated. For shorter-duration events (<6 h), average precipitation intensity scaling is in line with the expected Clausius–Clapeyron (CC) relation at ~7% $°C^{-1}$, and this decreases with increasing duration, down to 2% $°C^{-1}$ at 24-h duration. Consistent with climate scaling derived from model projections, 1-h peak precipitation intensities are found to increase with temperature at elevated rates compared to average precipitation intensities, with super-CC scaling (10%–14% $°C^{-1)}$ found for short-duration events in tropical climates.

SIGNIFICANCE STATEMENT: Deviating from theoretical and modeled projections of systematic increases in extreme precipitation intensities (climate scaling), decreasing rainfall intensities are commonly reported at higher temperatures in observational studies of extreme precipitation–temperature sensitivity (apparent scaling). Here we attribute this second-order discontinuity, or "hook" structure, to a decrease in the duration of precipitation events at higher temperatures, and not to a decrease in precipitation intensities. By incorporating precipitation duration into event-based apparent scaling analyses, we show improved spatial and temporal consistency of apparent scaling results. We find average precipitation intensities increase with temperature across all event durations and locations investigated, while 1-h peak intensities are increasing at elevated rates. Our results suggest increased precipitation intensities in a future warmer climate.

KEYWORDS: Australia; Extreme events; Precipitation; Rainfall; Climate classification/regimes; Climate sensitivity; Surface temperature; Regression analysis

1. Introduction

Extreme precipitation events that produce hazardous floods are generated by several complex and chaotic processes that are all susceptible to unequivocal atmospheric warming. The expected increase in future extreme precipitation intensities is primarily based on the increase in atmospheric saturation vapor pressure as a function of temperature, governed by the Clausius–Clapeyron (CC) relation, at a rate of ~7% $°C^{-1}$ at Earth's surface. Multimodel global climate change simulations have indicated a global rate of change of 7.4% $°C^{-1}$ for column water vapor, and 5.9% $°C^{-1}$ for surface specific humidity with respect to global-mean surface air temperature; however, strong deviations exist based on latitude and expression of rates in terms of global or local-mean surface temperatures (O'Gorman and Muller 2010). Model-predicted changes to global mean precipitation suggest increasing rates below CC (~2% $°C^{-1}$) (Held and Soden 2006; Mauritsen and Stevens 2015), while extreme precipitation generally increases at rates above CC (super-CC), particularly in tropical and subtropical regions (Emori and Brown 2005; Sugiyama et al. 2010). However, very large intermodel disagreements and poorly represented rain-rate distributions reduces confidence in the projected changes in extreme precipitation, suggesting some physical mechanisms at shorter time scales are not well represented (Allan and Soden 2008; Kharin et al. 2007; Peleg et al. 2018).

With large uncertainty around understanding changes to precipitation extremes in a warming climate (Fowler et al. 2021a,b; Kim et al. 2020; Westra et al. 2014), much research has focused on estimating local daily or subdaily extreme precipitation–temperature sensitivities based on observed climate records—referred to as "apparent scaling" in the scientific literature (Bao et al. 2017). Apparent scaling results can potentially provide improved understanding and estimation of

Supplemental information related to this paper is available at the Journals Online website: https://doi.org/10.1175/JCLI-D-21-0292.s1.

Corresponding author: Ashish Sharma, a.sharma@unsw.edu.au

DOI: 10.1175/JCLI-D-21-0292.1

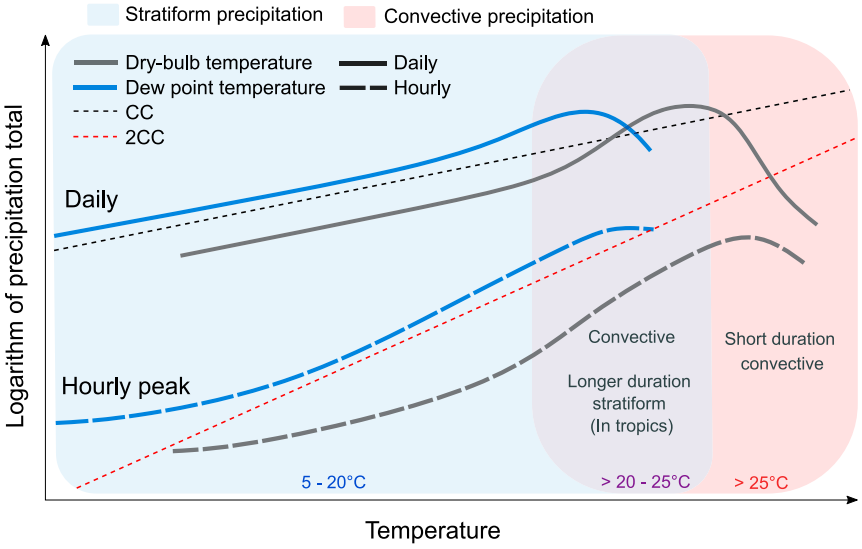

FIG. 1. Schematic of the influence of precipitation type and duration on apparent scaling of high-percentile extreme precipitation intensities with near surface dry-bulb and dewpoint temperature. At lower temperatures (5°–20°C), predominant stratiform precipitation produces daily and hourly curves close to CC scaling of 7% $°C^{-1}$ for both dry-bulb and dewpoint temperature. At higher temperatures (20°–25°C), a mixture of convective and stratiform precipitation events results in steeper hourly curves for both temperature variables, close to 2CC (twice the CC rate). This increase in apparent scaling rates also occurs in daily curves, although at a limited and higher temperature range compared to hourly curves. At the highest temperatures (>25°C), associated with predominantly short-duration convective storms, a strong decrease in daily dry-bulb scaling rates produces a hook-shaped curve, with a lessened hook shape for the daily dewpoint curve. Hourly curves at the highest temperatures undergo a less severe reduction in scaling rates, with a more pronounced hook developing for the dry-bulb curve compared to dewpoint temperature.

changes in future extreme precipitation through higher confidence temperature and atmospheric moisture projections—referred to as "climate scaling" (Bao et al. 2017; Lenderink and Attema 2015). However, apparent scaling has been found to vary significantly across the world (Fowler et al. 2021b), including substantial discrepancies between apparent scaling and climate scaling results (Bao et al. 2017; Sun et al. 2020; Zhang et al. 2017).

In cooler climatic regions, apparent scaling of daily precipitation totals is generally in line with the expected CC relation. However, in warmer climatic regions, negatively apparent scaling is commonly reported (Ali et al. 2018; Utsumi et al. 2011). This is in contrast to long-term trends in observed annual maximum daily precipitation are estimated to be between 5.9% and 7.7% $°C^{-1}$ of globally averaged near-surface atmospheric temperature, with greater rates of change in the tropics (Westra et al. 2013). At a subdaily scale, super-CC (>7% $°C^{-1}$) apparent scaling has been observed at multiple locations for hourly precipitation extremes (Lenderink and van Meijgaard 2008; Lenderink et al. 2011; Wasko et al. 2018). Apparent scaling relationships have been found dependent on a multitude of factors, including season (Berg et al. 2009; Wasko and Sharma 2014), convective versus stratiform precipitation type (Berg et al. 2013; Molnar et al. 2015), and choice of temperature-scaling variable (Ali and Mishra 2017; Bui et al. 2019; Golroudbary et al. 2019). Results are further complicated by the diverse methodological approaches in use (Zhang et al. 2017), which includes sensitivity to the timing and temporal resolution of the temperature sampling period (Visser et al. 2020). The reliability of apparent scaling as a basis for projecting future precipitation extremes has thus been questioned (Sun et al. 2020; Zhang et al. 2017).

Referring to Fig. 1, extreme precipitation intensities generally exhibit a monotonic increase with temperature before leveling off (upper-limit structure) or decreasing (peaklike or hook structure) at some threshold temperature (Panthou et al. 2014; Utsumi et al. 2011; Yin et al. 2021). A key influencing factor on the structure of extreme precipitation–temperature relationships is the accumulation period of the precipitation intensity, where elevated monotonic apparent scaling rates are typically found for subdaily precipitation (dotted line) extremes and peaklike structures for daily extremes (solid line) (Haerter et al. 2010; Hardwick Jones et al. 2010; Lenderink and van Meijgaard 2008; Westra et al. 2014).

Daily apparent scaling tends to follow CC over low to moderate temperature ranges (5°–20°C), while neutral/negative rates are associated with higher temperatures ranges (>20°–25°C) (Hardwick Jones et al. 2010; Wang et al. 2017). Strong negative daily apparent scaling is commonly found in warmer climatic regions, such as the tropics (>25°C), contradicting the expected

increase in precipitation intensities with higher temperatures (Ali et al. 2018; Maeda et al. 2012; Utsumi et al. 2011; Wasko et al. 2016). Compared to daily extremes, subdaily extremes tend to exhibit stronger (more positive) apparent scaling rates at low to moderate temperature ranges, with super-CC (>7% $°C^{-1}$) scaling of hourly extremes observed at multiple locations (Lenderink et al. 2011; Park and Min 2017; Schroeer and Kirchengast 2017; Wasko et al. 2015; Xiao et al. 2016). However, at higher temperature ranges (>20°–25°C), hourly extremes exhibit similar downward trends in scaling rates as daily extremes, although to a reduced extent (Hardwick Jones et al. 2010; Lenderink et al. 2011). Weaker (lower) daily apparent scaling rates, compared to subdaily scaling, have been attributed to the complex interplay of atmospheric process required to sustain long-duration precipitation (Lenderink and van Meijgaard 2008) and the underestimation of daily extremes due to increased precipitation intermittency (Lenderink et al. 2018; Schleiss 2018).

The hook structure at higher temperatures resulting in negative apparent scaling has primarily been attributed to lower moisture availability (Barbero et al. 2018; Berg et al. 2009; Fowler et al. 2021b; Hardwick Jones et al. 2010; Lenderink et al. 2018; Roderick et al. 2020), leading to the preference for dewpoint temperature, a measure of moisture, as the temperature-scaling variable. Improved consistency of dewpoint temperature-based scaling across temperature ranges has been framed alongside improved process understanding, with the identification of dewpoint temperature as the primary driver of precipitation extremes (Barbero et al. 2018). Dry-bulb temperature has also been shown to be the primary driver of short-duration extreme precipitation variability, contrary to dewpoint temperature-based findings, due to biases introduced through the event selection and temperature sampling (Visser et al. 2020). As a result, apparent scaling calculated using dewpoint temperature still often appear inconsistent with observations and model studies (Wasko and Nathan 2019; Zhang et al. 2019), with negative daily scaling in the tropics (Ali et al. 2018; Wasko et al. 2018) and super-CC hourly scaling across the majority of the globe (Ali et al. 2021).

Restricted by historical subdaily precipitation and temperature data availability, a limited number of studies have contributed to improved understanding of deviations of apparent scaling relationships from the expected CC relation across temporal scales. Stronger negative daily apparent scaling (stronger hook shape) compared to subdaily scaling at higher temperatures has been attributed to the complex interplay of multiple atmospheric phenomena (Drobinski et al. 2016; Lenderink and van Meijgaard 2008), including a reduction in accumulated precipitation due to decreasing the duration of rainfall events (or wet-time fraction) (Haerter et al. 2010; Schleiss 2018; Utsumi et al. 2011). A rapid decline in apparent scaling rates with precipitation durations greater than 30 min, has also suggested that expected CC scaling only applies to individual storm cells (Hardwick Jones et al. 2010). Short-duration convective events occurring at higher temperatures (see Fig. 1) might induce high rainfall rates, but the total rainfall accumulated over a longer time scale, such as one day, are likely to be less than a longer-duration stratiform event. The observed decrease in the extreme precipitation totals at high temperatures could therefore be due to the shorter duration of the precipitation event, and not to the decrease in precipitation intensity of the individual event (Haerter et al. 2010). However, this is yet to be proven. Indeed, investigating peak hourly extremes, Wasko et al. (2015) showed that negative apparent scaling in tropical regions of Australia can be reduced/reversed by conditioning the precipitation–temperature relationship on event duration but failed to find significant positive scaling for higher precipitation percentiles in tropical locations and longer durations.

Event duration is a precipitation event characteristic that is not easily extracted from readily available daily precipitation data. The primary event characteristic of interest in apparent scaling analyses is usually the accumulated precipitation over a selected time period. Precipitation totals in apparent scaling methods are typically aggregated using one of the following two approaches: (i) period based (also referred to as duration based), where total precipitation is accumulated over a set duration, for example, 1 day; or (ii) event based, where independent precipitation events are selected using a minimum interevent time (MIT) and precipitation depth criteria, with precipitation accumulated over the duration of the precipitation event (referred to as event duration). However, with period-based approaches, there is a loss of information on the (physical) relationship between the temperature driving the precipitation, as well as on the precipitation event itself. On the other hand, event-based approaches have been shown to provide apparent scaling results in line with the expected CC value for 1-h peak precipitation intensities when paired with temperature sampled before the start of the precipitation event (Visser et al. 2020). In addition, the use of event-based approaches provides a promising line of investigation as they preserve the characteristics of the precipitation event, allowing for conditioning on event attributes, such as event duration.

This leads us to the central research questions in this study:

1) Is decreasing/negative apparent scaling at higher temperatures is a result of a decrease in the duration of the precipitation event and not the decrease of the rainfall rate of the individual storm?
2) Are apparent scaling rates more consistent with theoretical and modeled predictions across temporal and spatial ranges when conditioned on event duration?

We use a continentwide dataset that encompasses a wide variety of climates (and hence temperature ranges) covering all parts of the apparent scaling curve (Fig. 1). Conditioning an event-based approach on duration, we demonstrate decreasing/negative apparent scaling rates at higher temperatures is the result of decreasing precipitation yield associated with decreasing event duration, explaining stronger hook structures for larger precipitation accumulation periods such as daily. This finding enables us to develop a standardized pooling approach for station data across climate zones, allowing for a more stable analysis of apparent scaling across various event durations, which shows systematic, consistent, positive apparent scaling in line with theoretical and modeled predictions.

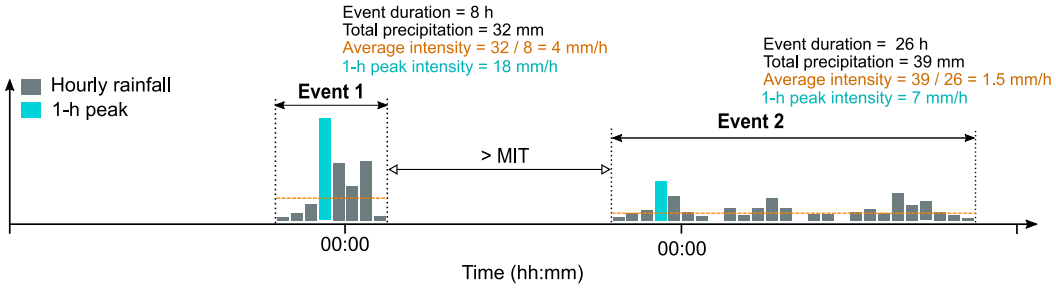

FIG. 2. Rainfall event selection using an event-based approach and MIT with calculated rainfall characteristics per event.

2. Data and methods

a. Meteorological data

Quality controlled data were obtained from the Australian Bureau of Meteorology. Precipitation is measured using either Dines tilting syphon pluviographs or tipping-bucket rain gauges (TBRGs) at 6-min intervals and is available for 1489 stations across Australia. Precipitation data marked as ''value has been estimated through linear interpolation'' were dismissed. Subdaily dry-bulb temperature (referred to hereon as temperature) and dewpoint temperature measurements are available from 1829 and 1574 synoptic stations, respectively, where recording resolution varies from 2 to 8 measurements a day. Due to the low precision (0 decimals) of many dewpoint temperature records, higher precision records were constructed using actual vapor pressure derived from psychrometric data as described by Visser et al. (2020). Analysis was restricted to sites that have >10 years of record and with <25% missing data, yielding 385 qualifying stations distributed across Australia, 250 of which had dewpoint temperature records reconstructed from actual vapor pressure.

b. Selection of rainfall events

During the Australian Bureau of Meteorology's nationwide rainfall gauge transition from pluviographs to TBRGs in 1995, the threshold for recording precipitation consequently increased from 0.01 mm (pluviograph) to 0.2 mm (one tip for TBRG). Unlike pluviographs, trace amounts of rainfall (<0.2 mm) per measurement interval do not register in TBRG records, as only filled bucket tips (0.2 mm) are measured. Increased periods of zero precipitation are consequently observed in TBRG records compared to pluviographs, resulting in discrepancies over time in such rainfall event attributes such as event intermittency, event duration, and frequency of events. To ensure consistency in rainfall event attributes across differing gauge records, pluviographs records were converted to TBRG records by emulating TBRG operation. Two rainfall events were considered independent if they were separated by at least 3-h of zero precipitation. A MIT of 3-h is selected as a balance between ensuring independence of events and the need to limit intraevent intermittency (Gaál et al. 2014; Wasko et al. 2015). A reduction/increase in the selected MIT will affect derived event durations due to the reduction/increase in precipitation event intermittency, potentially impacting results. The sensitivity of results was tested by varying the selected MIT from 1 to 5 h, which indicated limited variability in resultant scaling rates. However, the systematic reduction in the number of longer-duration events with the use of shorter MITs, can increase scaling variability in data-poor regions. Events with an average precipitation intensity of less than or equal to 0.2 mm h^{-1} were omitted. Events with very short durations, less than or equal to 18 min, were also omitted.

c. Precipitation–temperature pairs

The 1-h peak precipitation intensity was extracted for each selected rainfall event (Fig. 2). With increasing event durations, short-duration extremes such as the 1-h peak intensity become a smaller contributing percentage to the total event precipitation. Apparent scaling results of 1-h peak precipitation extremes consequently provide limited information on potential changes to precipitation rates across longer-duration events. Therefore, the average precipitation intensity of each selected event was calculated as the total event precipitation divided by the event duration (Fig. 2). Both the average intensities and 1-h peak intensities were matched to the mean temperature and dewpoint temperature sampled over the 24-h period before the start of the precipitation event using subdaily temperature data. This sample period has been found to be indicative of precipitation variability while minimizing the impacts of the cooling effect of the rainfall event itself (Visser et al. 2020).

d. Scaling calculation for individual stations

Apparent scaling of precipitation–temperature pairs was calculated using quantile regression (Koenker and Bassett 1978), which has been shown to produce more robust and unbiased scaling estimates compared to binning techniques (Wasko and Sharma 2014), referred to as ''binning scaling'' (Sun et al. 2020; Zhang et al. 2017). Quantile regression was undertaken using the R package ''quantreg'' (Koenker 2018), with the scaling of peak precipitation intensity (P) with temperature (T) calculated using Eq. (1):

$$\log(P) = \beta_0^q + \beta_1^q T, \tag{1}$$

where q is the selected quantile, and β_0 and β_1 are fitted parameters. The scaling (α) of precipitation intensity with

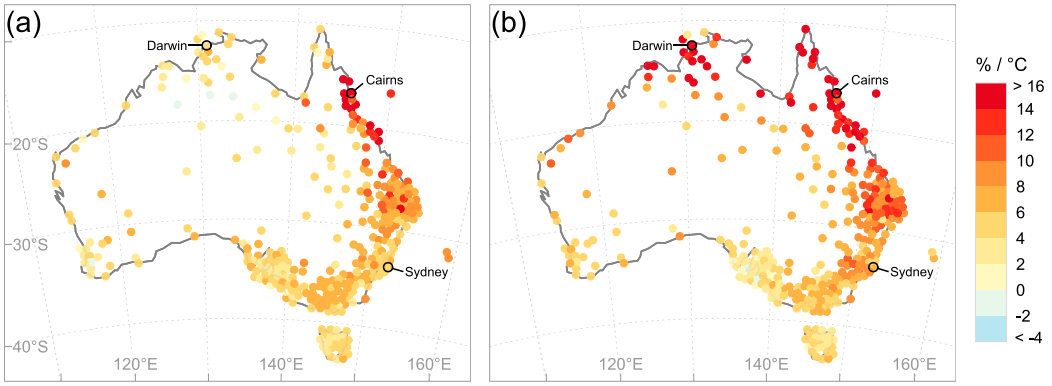

FIG. 3. Scaling of 95th-percentile (a) 1-h peak precipitation intensity and (b) average precipitation intensity to dry-bulb temperatures across Australia. Minimum requirement of 500 events per station. Darwin Airport (ID 014015), Cairns Airport (ID 031011), and Sydney Observatory (ID 66062) stations indicated as Darwin, Cairns, and Sydney.

temperature as a percentage was calculated through an exponential transformation of the slope of the fitted quantile regression relationship, β_1^q, using Eq. (4):

$$P = e^{\beta_0^q} \times \left(e^{\beta_1^q}\right)^T, \tag{2}$$

$$P = e^{\beta_0^q} \times (1+\alpha)^T, \quad \text{and} \tag{3}$$

$$\alpha = e^{\beta_1^q} - 1 \tag{4}$$

such that $\alpha = 0.07$ is equivalent to CC-like scaling of 7% $°C^{-1}$.

e. Scaling calculation for pooled data

Precipitation–temperature pairs were standardized (z scores) per station using Eq. (5):

$$z = \frac{X - \mu}{\sigma}, \tag{5}$$

where X is the observed temperature or precipitation intensity transformed into the logarithmic domain, μ its sample mean, and σ its sample standard deviation. After standardization, precipitation–temperature pairs are pooled across climate zones according to the Köppen–Geiger classification system (Beck et al. 2018). The fitted quantile regression relationship, β_4^q, in Eq. (6) has a unit of $\sigma_{\log(P)}/\sigma_T$ and the scaling (α) of the pooled sample can be calculated using Eq. (7):

$$z_{\log(P)} = \beta_3^q + \beta_4^q z_T \quad \text{and} \tag{6}$$

$$\alpha = e^{\beta_4^q} - 1 \times \left(\frac{\sigma_{\log(P)}}{\sigma_T}\right), \tag{7}$$

where $\sigma_{\log(P)}/\sigma_T$ is calculated from the pooled sample.

f. Aggregation to daily data and binning

To demonstrate the elimination of the stronger hook structures in daily precipitation–temperature relationships (compared to hourly precipitation–temperature relationships), a binning technique was employed. Compared to quantile regression, which produces a single scaling estimate over a defined temperature range, binning techniques allow for greater examination of precipitation variations within a temperature range. Daily precipitation totals and daily mean temperatures were aggregated based on subdaily data, with the daily start time taken as 0900 local time. Daily precipitation totals were paired to the mean temperature of the same day. Daily precipitation percentiles (95th and 99th) were calculated at the center of a rolling 1.5°C temperature bin at 1°C intervals across the applicable temperature range (minimum requirement of 100 data pairs per bin).

3. Results

a. Scaling of 1-h peak intensities versus average intensities

Figure 3 provides a comparison between the apparent scaling for the 95th nonexceedance percentile 1-h peak precipitation intensity and average precipitation intensity for stations

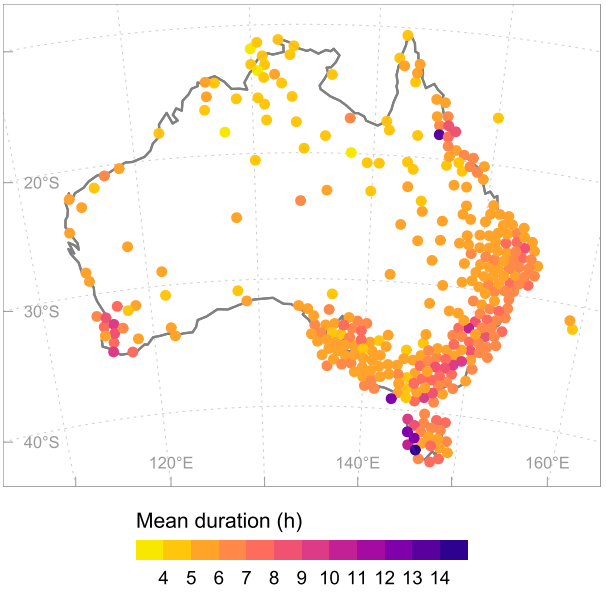

FIG. 4. Mean precipitation event duration for stations across Australia based on a minimum interevent time of 3 h.

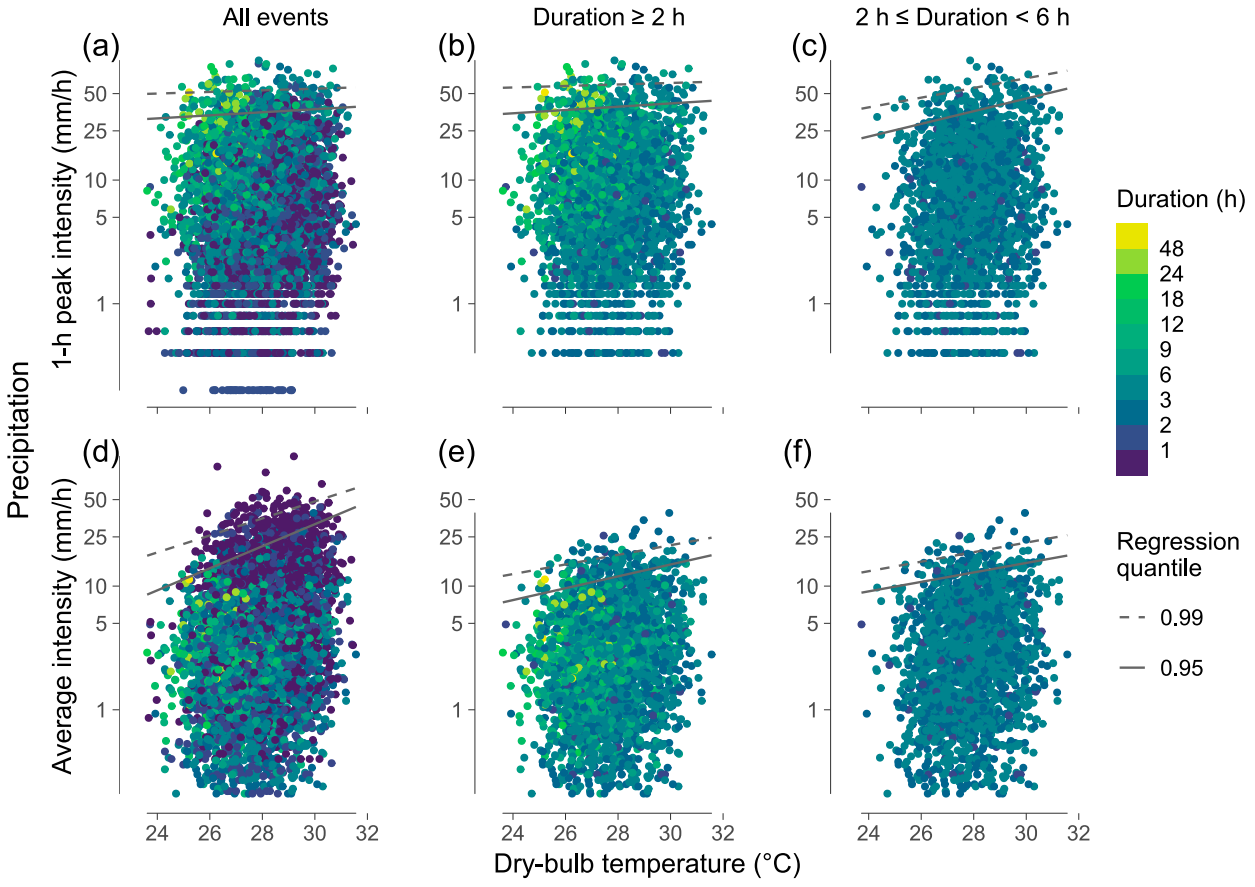

FIG. 5. Precipitation intensity vs dry-bulb temperature for Darwin Airport station (ID: 014015): (a)–(c) 1-h peak precipitation intensity and (d)–(f) average precipitation intensity. Results are presented based on event duration subsets: (a),(d) all events; (b),(e) greater than 2 h; (c),(f) between 2 and 6 h. Quantile regression lines presented for the 95th and 99th nonexceedance percentiles.

across Australia. Peak 1-h intensities (Fig. 3a) show positive apparent scaling rates for almost all stations, with a neutral to slight negative scaling rates observed for a small number of northern inland stations. Scaling rates along the southern and eastern coastlines are close to the expected CC of 7% $°C^{-1}$, with slightly elevated values for the central east coast. Extraordinary high scaling rates (>16% $°C^{-1}$) are observed for a small stretch of the tropical northeastern coastline (surrounding Cairns in Fig. 2), while low positive scaling rates (<7% $°C^{-1}$) are observed along northern coastal and inland regions (surrounding Darwin in Fig. 2).

Apparent scaling for average precipitation intensities (Fig. 3b) is considerably higher along the northern regions of Australia compared to 1-h peak intensities. Comparable rates are found in the southern half of the country, with slightly elevated average intensity apparent scaling rates along the southeastern coastline. The clear mismatch between apparent scaling rates of 1-h peak precipitation intensities and average precipitation intensities in the tropical north of the country is unexpected, as 1-h peak intensities within precipitation events are expected to scale at roughly comparable rates to average intensities. Previous studies have found negative apparent scaling for 1-h peak intensities in the northern regions of Australia (Hardwick Jones et al. 2010; Wasko et al. 2015), which would suggest even greater discrepancies with indicated average precipitation intensity scaling.

The tropical north of Australia is a region with higher mean temperatures and annual precipitation compared to the rest of the country. However, due to the dominant tropical convective activity over the wet (summer) season, mean event durations are markedly shorter than those in the southern (more temperate) regions (Fig. 4), resulting in high average precipitation intensities. To understand why this mismatch between the 1-h peak and average intensity apparent scaling occurs in this region, Fig. 5 presents a detailed comparison of apparent scaling for Darwin Airport station (ID 014015), located on the north coast of Australia as indicated in Fig. 3. Average precipitation intensities and 1-h peak precipitation intensities for Darwin rainfall events are plotted against their paired temperature, where each of the peak precipitation–temperature pairs are colored by their associated event duration. The impact of duration conditioning is investigated through adopting increasingly stringent subsets on event duration to isolate events of similar length (Figs. 5b,c,e,f).

Comparison of 1-h peak precipitation intensity (Fig. 5a) and average precipitation intensity (Fig. 5d) apparent scaling

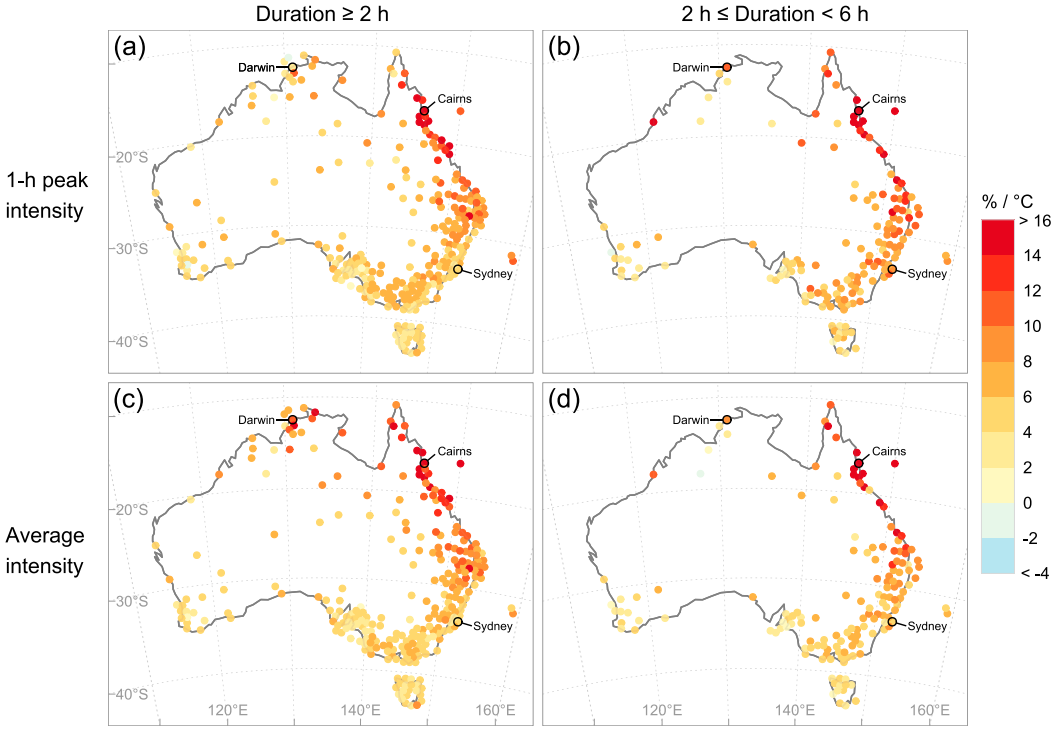

FIG. 6. Scaling of 95th-percentile (a),(b) 1-h peak precipitation intensity and (c),(d) average precipitation intensity to dry-bulb temperature across Australia. Results are presented based on event duration subsets: (a),(c) greater than 2 h; (b),(d) between 2 and 6 h. Minimum requirement of 500 events per station. Darwin Airport station (ID: 014015) indicated as Darwin.

results for all rainfall events reveals the mismatch of slight positive scaling for 1-h peak precipitation intensities to strong positive scaling of average precipitation intensities as indicated in Fig. 3. The color coding of event durations reveals a dominance of shorter-duration events (darker green to blue) at higher temperatures, with the occurrence of less prominent longer-duration events (light green to yellow) at lower temperatures. Events with durations less than 1 h (darkest blue) typically have lower 1-h peak intensities compared to longer-duration events, as there is a greater probability of a continuous 1 h of precipitation occurring in a longer-duration event. This bias toward longer-duration events grows stronger with increasing accumulation periods, for example, assessing the 2-h peak intensity within an event (Fig. S1 in the online supplemental material) or daily rainfall totals. This is because (i) most events have a duration significantly smaller than the selected accumulation period, and (ii) there is an increased probability of continuous period of heavy precipitation occurring within a longer-duration event.

Longer-duration events require sustained moisture inflow typically brought on by large-scale circulation systems, strong monsoon development or cyclones, all associated with cooler temperatures. The combined analysis of these longer-duration events, with shorter-duration convective based storms at higher temperatures, increasingly contribute to reduced scaling with increasing accumulation periods. Results for Sydney Observatory station (ID 066062) (Fig. S2) located on the temperate southeast coast of Australia, reveal greater consistency between apparent scaling rates of 1-h peak intensities and average intensities. This is due to the greater uniformity in the distribution of event durations across a wider and lower temperature range. For Darwin, limited longer-duration events (>12 h) occur at temperatures above 28°C. This highlights how regional- or site-specific studies may overlook variability in the apparent scaling presented in Fig. 1 due to a limited temperature range.

Accurately assessing changes in peak intensities with temperature, particularly in warmer climates, requires a more direct comparison of rainfall events with durations greater than the accumulation period under investigation, ideally with durations similar in length (similar storm mechanisms). To ensure event durations are sufficiently longer than the peak 1-h accumulation period in question, we subset on events with durations greater than 2 h (Figs. 5b,e) to find improvement in consistency between peak and average precipitation intensities for Darwin. Average precipitation intensity apparent scaling (Fig. 5e) is significantly reduced with removal of more intense short-duration rainfall bursts. Isolating events of similar durations between 2 and 6 h (Figs. 5c,f) reveals comparable positive scaling for average precipitation intensities and 1-h peak intensities, and hence we extend this analysis countrywide (Fig. 6).

Restricted to events greater than 2 h in duration, a countrywide comparison reveals the mismatch between apparent scaling

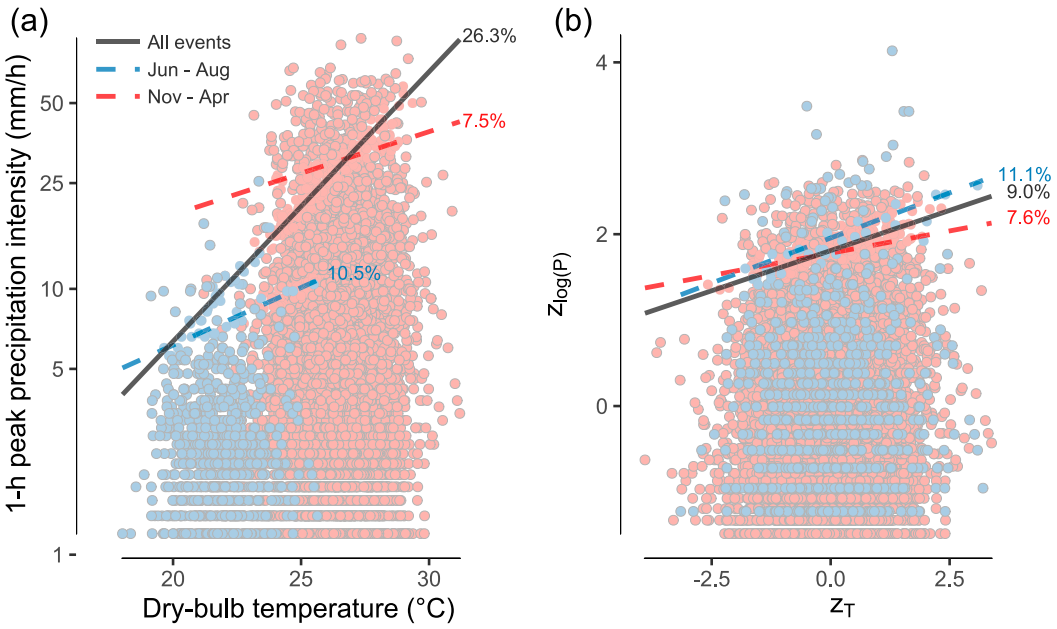

FIG. 7. Scaling of 95th-percentile 1-h peak precipitation intensity to dry-bulb temperature for Cairns Airport station (ID: 031011) for (a) nonstandardized and (b) standardized precipitation–temperature pairs. Scaling results are presented for all events and seasonal subsets based on the high-rainfall (November to April) and low-rainfall (June to August) seasons.

rates of 1-h peak precipitation intensities (Fig. 6a) and average precipitation intensities (Fig. 6c) is concentrated around northern tropical regions. Subsetting for event durations between 2 and 6 h (Figs. 6b,d) results in improved consistency between the apparent scaling of 1-h peak precipitation intensities (Fig. 6a) and average precipitation intensities (Fig. 6d) across the country; however, this highlights the immense reduction in qualifying stations due to the reduced number of events available per analysis. Narrower event durations subsets, such as between 2 and 3 h, will likely further improve consistency of results through greater isolation of temperature influence on precipitation intensities. However, the reduction of available events per analysis dramatically decreases with increasing event durations and narrower subsets.

b. *Pooling of station data across climate zones*

Analyzing longer-duration events is limited by station data availability, particularly in regions with storm mechanisms that predominantly yield short-duration events. The number of available events per analysis can be increased in two ways: 1) relaxation of narrow event duration subsets, or 2) pooling of station data across similar climatic regions. As the relaxation of event duration subsets contributes to reduced apparent scaling (section 3a), pooling is required to increase the size of the samples considered. Accordingly, the precipitation–temperature pairs were pooled across climatic regions based on the Köppen–Geiger climate classification system (see section 2e).

Pooling approaches have been adopted in previous manuscripts (Ali et al. 2021; Utsumi et al. 2011); however, precipitation and temperature data were not standardized before pooling, which can introduce the artifact of super-CC scaling (Molnar et al. 2015). Pooling of nonstandardized data across stations with significant differences in precipitation and temperature distributions can produce artificially high combined scaling that exceeds the scaling at individual stations. An example of this is presented for Cairns Airport station (ID 031011) (Fig. 7) where strong seasonality in event precipitation totals and mean temperatures produces a combined scaling rate that exceeds that of the individual seasons (Fig. 7a). This is a similar situation to elevated scaling produced by the combined analysis of two different precipitation mechanisms (Fig. 1). Two seasons (two dominant storm mechanisms) or two individual stations can individually exhibit near-CC scaling (10.5% and 7.5% $°C^{-1}$). But a combined analysis of data pools with distinct differences in mean precipitation intensity and temperature, can result in greater scaling than the two individual seasons or stations, in this case 26.3% $°C^{-1}$. Standardization of precipitation–temperature before pooling (Fig. 7b) retains individual scaling rates and allows for combined scaling estimate that is not artificially inflated due to precipitation and temperature discrepancies. In this case the average of the individual of the two stations or seasons combined is 9% $°C^{-1}$ as expected.

c. *Apparent scaling across event duration and region*

Figures 8 and 9 present the apparent scaling for the 95th-percentile average precipitation intensity (Fig. 8) and 1-h peak intensity (Fig. 9) across event durations for data pooled (and standardized) using Köppen–Geiger climate classification. Three main climate types are represented with an initial capital letter: A (equatorial), B (arid), and C (warm temperate) groups. Seasonal precipitation subgroups (second letter) and temperature subgroups (third letter) provide further differentiation;

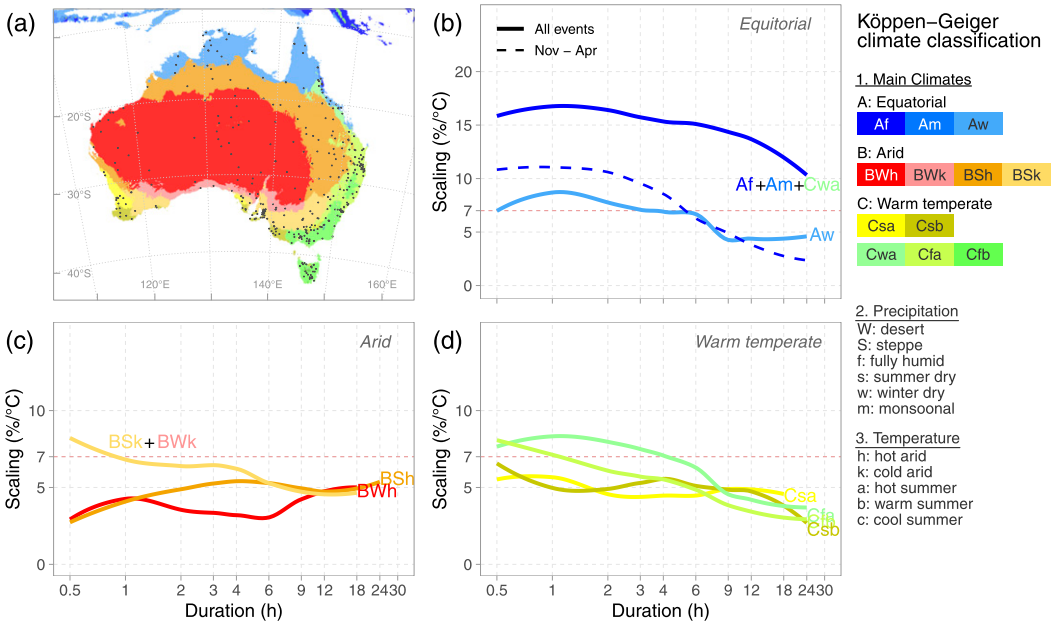

FIG. 8. Scaling of 95th-percentile *average precipitation intensity* to dry-bulb temperature across event durations for pooled stations per (a) Köppen–Geiger climate group for Australia (contributing stations indicated as black dots). Results are presented per main climate group for (b) A: equatorial; (c) B: arid; and (d) C: warm temperate. For a selected event duration value (x axis), the corresponding scaling rate is calculated based on a subset of precipitation events with durations between the selected and following event duration value, e.g., durations between 0.5 and 1 h. The Köppen–Geiger classification coverage was obtained from Beck et al. (2018) at 0.083° resolution. The color scheme was adopted from Peel et al. (2007). CC scaling at 7% °C^{-1} is represented by horizontal red dashed lines. Minimum requirement of 500 events per climate zone per duration subset.

however, due to limited station coverage, selected climate groups have been combined, including Af, Am, and Cwa along the northeast coastline and BSk and BWk along the southern inland region. Event duration subsets are selected based on the diverging objectives of isolating events by similar duration, while ensuring sufficient data points for analysis. For event durations smaller than 4 h, duration subsets are 1 h in width or smaller due to the high number of available events. With increasing event durations and decreasing events numbers, subset widths are increased to an upper duration limit of between 24 and 30 h.

Overall, across regions, near CC scaling is observed for shorter durations decreasing with increasing event duration. For equatorial climate groups (Fig. 8b), elevated scaling (>2CC) is evident for the combined group Af, Am, and Cwa, located along the northeast tropical coastline. As shown in Fig. 6, strong seasonality in event precipitation totals and mean temperatures for this region can produce combined scaling exceeding individual seasons. Subsetting on the high-rainfall season of November to April (dashed line) produces lower scaling (10.9% °C^{-1}), closer to the neighboring winter dry tropical climate group, Aw. For shorter event durations (<6 h), group Aw produces scaling close to CC. For longer event durations (>6 h), a downward trend in scaling rates can be seen for both equatorial groups while remaining positive. For arid regions (Fig. 8c), a similar scaling pattern to Aw is found for the combined arid group of BSk and BWk. Covering vast and diverse arid regions, groups BWh and BSh produce increasing scaling rates with event duration ranging from 2.7% to 5.6%. Increased variability in results for arid groups are likely due to limited station data availability across vast arid expanses. Warm temperate groups (Fig. 9d) scale at rates close to CC for shorter-duration events (<6 h), with a downward trend found for longer-duration events (>6 h)

The results in Fig. 8 presented a positive scaling for average precipitation intensity with temperature for all event durations analyzed. For the 1-h peak intensities within precipitation events (Fig. 9), scaling above average intensity rates are found for most climate groups. For equatorial groups (Fig. 9b), super-CC scaling (10%–14% °C^{-1}) is found for short-duration events, while reducing to 7% °C^{-1} at 24-h duration. For arid groups (Fig. 9c), scaling is found in line with CC, slightly elevated compared to average intensity rates. Comparable results are found for 1-h peak and average intensities across warm temperate groups (Fig. 9d), with increased distinction between lower scaling southern groups (Csa and Csb) and higher scaling southeastern coastal groups (Cfa and Cfb). Comparison of Figs. 8 and 9 reveals similar downward trends in scaling rates for longer event durations. With increasing event durations, the 1-h peak intensity contributes a deceasing portion of the total event precipitation and is likely comparable across longer event durations, contributing to reduced scaling.

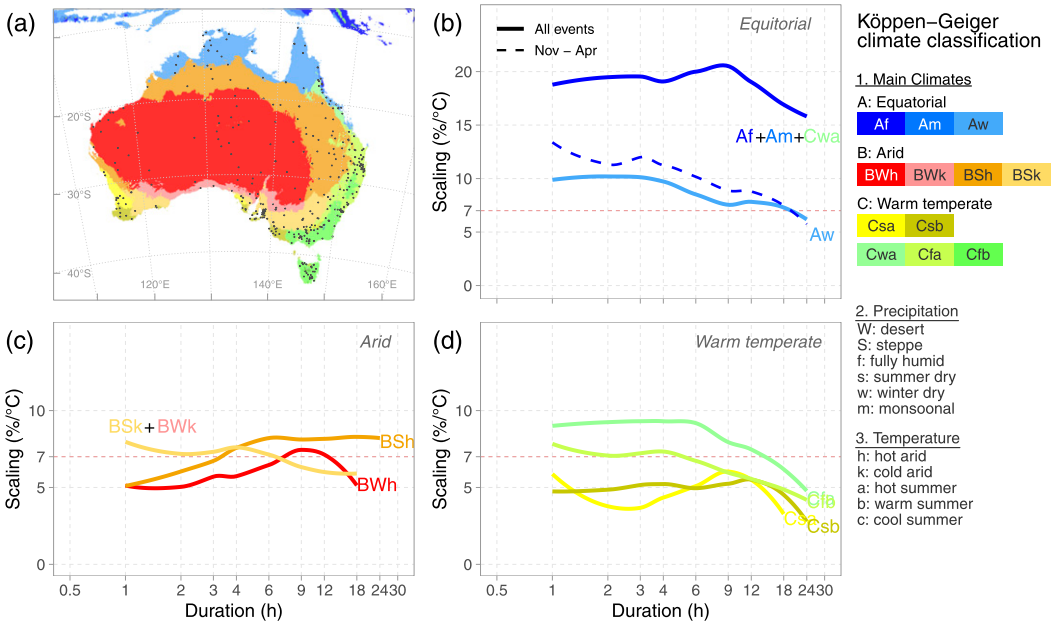

FIG. 9. Scaling of 95th-percentile *1-h peak precipitation intensity* to dry-bulb temperature across event durations for pooled stations per (a) Köppen–Geiger climate zone for Australia. The format of the figure is as in Fig. 8.

d. *Addressing stronger hook structures in daily apparent scaling*

Preceding result subsections have indicated that duration subsetting can increase neutral/low scaling of 1-h peak intensities at higher temperatures (Fig. 5). However, as most precipitation events at higher temperatures are short in duration and low in daily precipitation total, extreme precipitation–temperature relationships for daily precipitation totals have generally exhibited a much stronger hook structure compared to 1-h peak intensities (Fig. 1). To investigate if duration conditioning can eliminate the strong negative apparent scaling for daily precipitation at higher temperatures, we examine the daily precipitation–temperature relationship for two stations in distinct climate zones, Sydney (temperate) and Darwin (equatorial) (Fig. 10), based on a binning technique (see section 2e). As daily precipitation totals do not capture event attributes such as duration, we condition daily precipitation totals (aggregated from subdaily data) on the percentage of 6-min subdaily intervals on which rainfall was measured or wet-time fraction (Figs. 10a,b). For comparison, the impact of duration conditioning on event-based precipitation totals is presented in Figs. 10c,d. It should be noted that for event-based precipitation totals (Figs. 10c,d), precipitation totals are accumulated over the event duration, which ranges from subdaily bursts to multiday events.

Figure 10a reveals a strong decrease in the wet-time fraction at higher temperatures for both Sydney and Darwin, with decreasing daily precipitation percentiles for drier days. Following a 7% $°C^{-1}$ increase in daily precipitation totals, Sydney develops a hook structure roughly around 20°C. For Darwin, a monotonic decrease in daily precipitation totals is evident, with a more distinct decrease in wet-time fraction across a narrow and elevated temperature range. A comparison of event-based precipitation totals (Fig. 10c) reveals greater neutral scaling behavior due to longer precipitation accumulations periods and paired temperature sampled before the start of the event. However, negative scaling is still observed at higher temperatures at both stations, with larger differences in 95th and 99th precipitation percentiles for Darwin attributed to large variations in event durations compared to a consistent daily time step.

Using the wet-time fraction as a surrogate for event duration, daily precipitation totals can be conditioned through subsets on wet-time fraction (Fig. 10b). This wet-fraction conditioning produces CC-like scaling for both stations across the entire temperature range, which is comparable to duration conditioning on event-based precipitation totals (Fig. 10d). Figure 10 reveals both daily and event-based apparent scaling can produce decreasing/negative apparent scaling rates across climate zones if the duration of precipitation is not considered. As subdaily precipitation data is required for the calculation of daily wet-time fractions, the use of event-based approach should be favored if subdaily data is available. This preference is based on the benefits offered by event-based methods over period-based methods, such as the extraction of precipitation event attributes and allowing for temperature sampling before the start of the event to minimize the cooling effect of the precipitation (Visser et al. 2020).

4. Discussion and conclusions

a. *Explaining negative apparent scaling at higher temperatures*

Previous studies have presented multiple conflicting reasons for decreasing/negative apparent scaling in warmer climatic regions. Investigating discrepancies in apparent scaling with

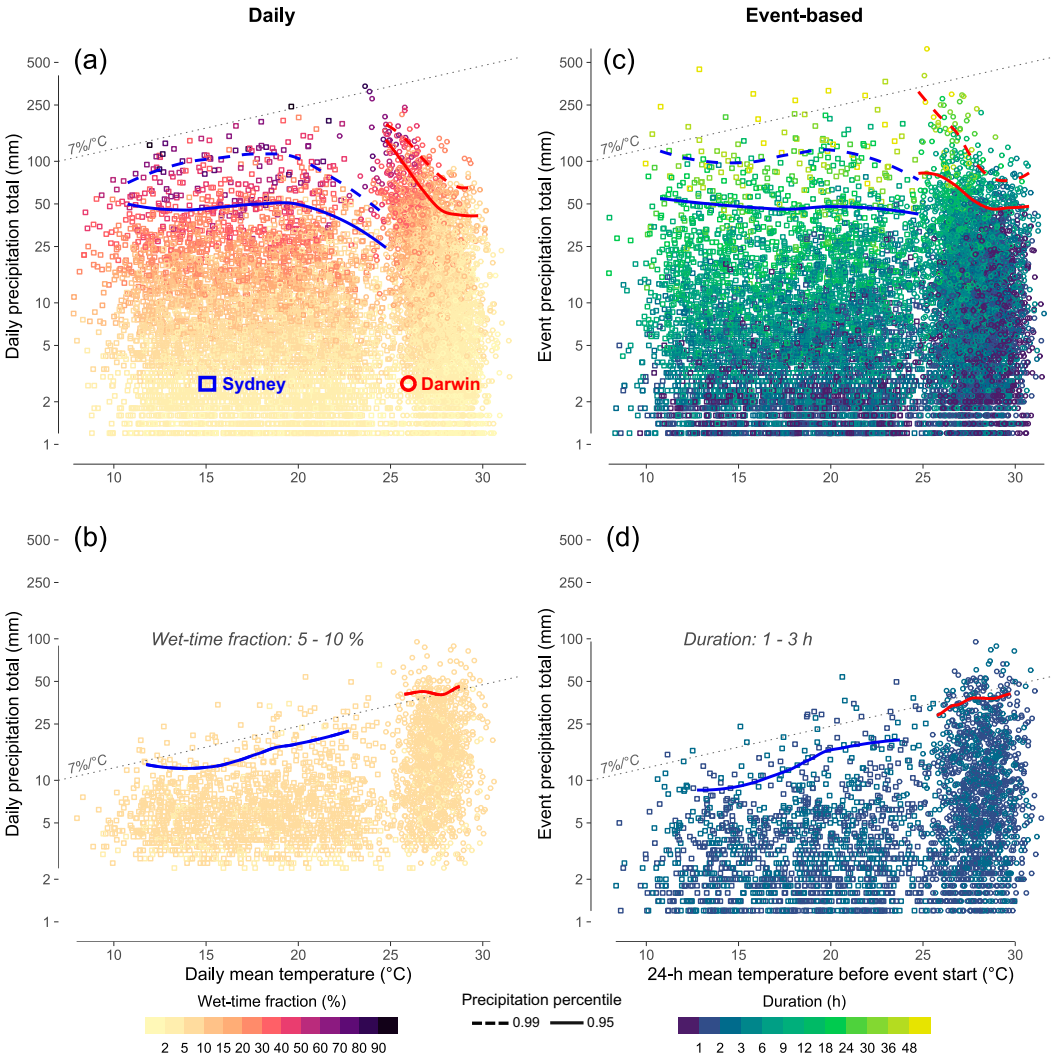

FIG. 10. (a),(b) Daily precipitation total vs dry-bulb temperature for Sydney (squares) and Darwin (circles), with (b) conditioning on wet-time fraction (5%–10%). (c),(d) Event precipitation total vs dry-bulb temperature for Sydney and Darwin, with (d) conditioning on event duration (1–3 h). Dotted (99th) and solid (95th) lines represent precipitation percentiles for Sydney (blue) and Darwin (Red) calculated based on 1.5°C-wide rolling temperature bins (minimum requirement of 100 events per bin).

increasing accumulation periods across Australia, we find the decreasing/negative apparent scaling (peaklike or hook structure) at higher temperatures is the result of a decrease in the duration of the precipitation event, and not the decrease of the precipitation rate of the individual event. This finding is in contrast to the prominent reasoning, which attributes negative apparent scaling at higher temperatures to lower moisture availability, while aligning with studies highlighting the influence of precipitation duration on discrepancies between daily and subdaily apparent scaling.

With increasing precipitation accumulation periods, such as hourly to daily, a greater portion of precipitation events are shorter in duration than the accumulation period in question, resulting in bias toward longer-duration events associated with cooler temperatures. But short-duration convective storms at higher temperatures produce lower rainfall totals compare to long-duration stratiform events over lengthy accumulation periods. This induces a negative apparent scaling, particularly in warmer climatic regions, such as the tropics. Greater uniformity in the distribution of event durations across a wider and lower temperature range in temperate climates, highlights how regional- or site-specific studies may overlook variability in the apparent scaling.

The development of stronger hook structures in the tropics can be attributed to a combination of the following three factors: 1) most events are short in duration (dominant convective mechanism), 2) mean event duration decreases strongly with increasing temperature, and 3) rainfall occurs within a narrow and elevated temperature range. Introduction of event duration subsetting allows for clearer identification of temperature's

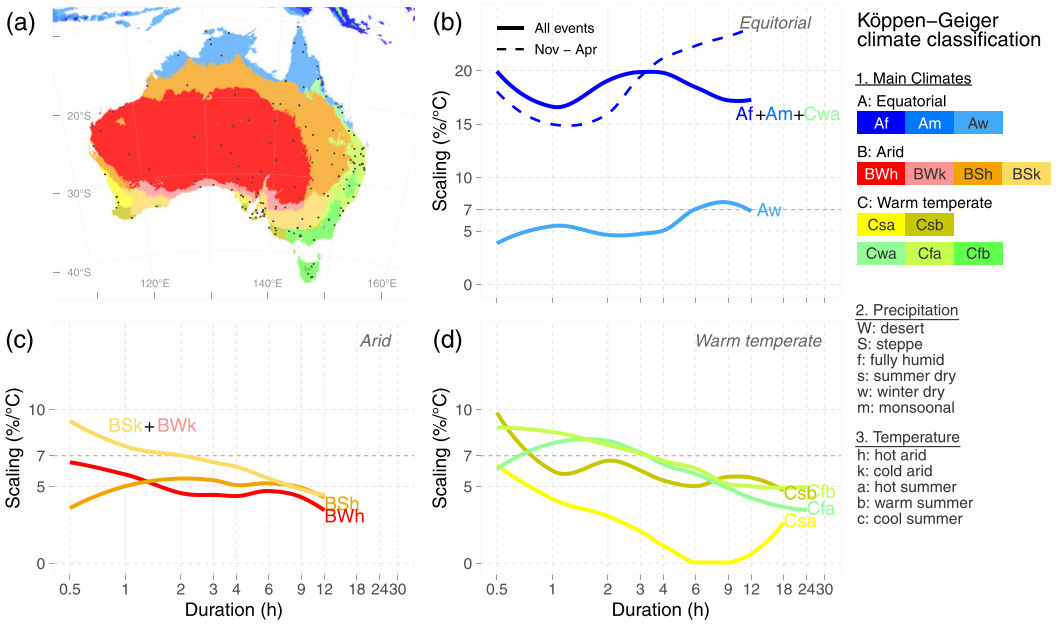

FIG. A1. As in Fig. 8, but for dewpoint temperature.

role in changes to precipitation intensities for specified event durations.

b. *Consistent positive apparent scaling across durations and climate zones*

Duration subsetting greatly reduces the number of available precipitation–temperature pairs available per analysis. Pooling of station data across regions of similar climatology can provide additional data pairs per duration subset; however, pooling of stations with substantial differences in temperature distributions and associated precipitation totals can lead to very high apparent scaling (>2CC). Standardization of precipitation–temperature pairs before pooling across climate zones produces results consistent with station-based analyses.

Pooling across Köppen–Geiger climate groups, we find average precipitation intensities increase with temperature across all event durations investigated (up to 30 h). For shorter-duration events (<6 h), scaling is in line with the expected CC value of 7% $°C^{-1}$, while rates decrease with increasing event durations (lowest value of 2.3% $°C^{-1}$ at 24–30 h). Peak 1-h precipitation intensities within events increase with temperature at marginally elevated rates compare to average precipitation intensities. For short-duration events, super-CC scaling (10%–14% $°C^{-1}$) for 1-h peak intensities is found in equatorial climates. These apparent scaling results of hourly extremes are consistent climate scaling obtained from convective permitting models over western Europe (Lenderink et al. 2021). A suggested physical mechanism leading to super-CC behavior in convective clouds is the enhancing convergence of moisture due to dynamical cloud feedbacks (Loriaux et al. 2013; Trenberth et al. 2003), with steeper temporal distribution of rain intensity observed at higher temperatures (Wasko and Sharma 2015). Scaling rates for average and 1-h peak precipitation intensities decrease with increasing duration, but notably remain positive.

c. *Dewpoint temperature as primary scaling variable*

The role of moisture availability was investigated with the reproduction of the precipitation–temperature sensitivities aggregated over climate zones using dewpoint temperature (see Figs. A1 and A2 in the appendix). Dewpoint temperature-based results appear largely consistent with dry-bulb temperature-based findings, with increased variability due to limited station data. This result is somewhat expected, as dry-bulb and dewpoint temperatures converge with increasing relative humidity at the onset of precipitation events. Notable exceptions in results include marginally increasing scaling rates with event duration for equatorial group Aw, both for average and 1-h peak intensities. However, exceedingly high scaling (>2CC) is found for combined equatorial group Af, Am, and Cwa, which could be attributed to greater variability induced by limited dewpoint temperature data for this region. For longer-duration events in group Aw, dewpoint temperature scaling is found closer to the expected CC value compared to lower dry-bulb temperature scaling. This result aligns with the physical reasoning that short-duration extremes can be better described by the atmospheric state before the storm, such as atmospheric stability, whereas for longer-duration events, not only is the precipitation rate important but also how long it can be sustained for, that is, requiring continuous moisture replenishment from large-scale atmospheric circulation (Lenderink et al. 2018). Due to the complexity of longer-duration events, additional climatic information such as the total moisture flux and precipitation efficiency over an event duration, will likely be required to advance our understanding of apparent scaling over longer durations.

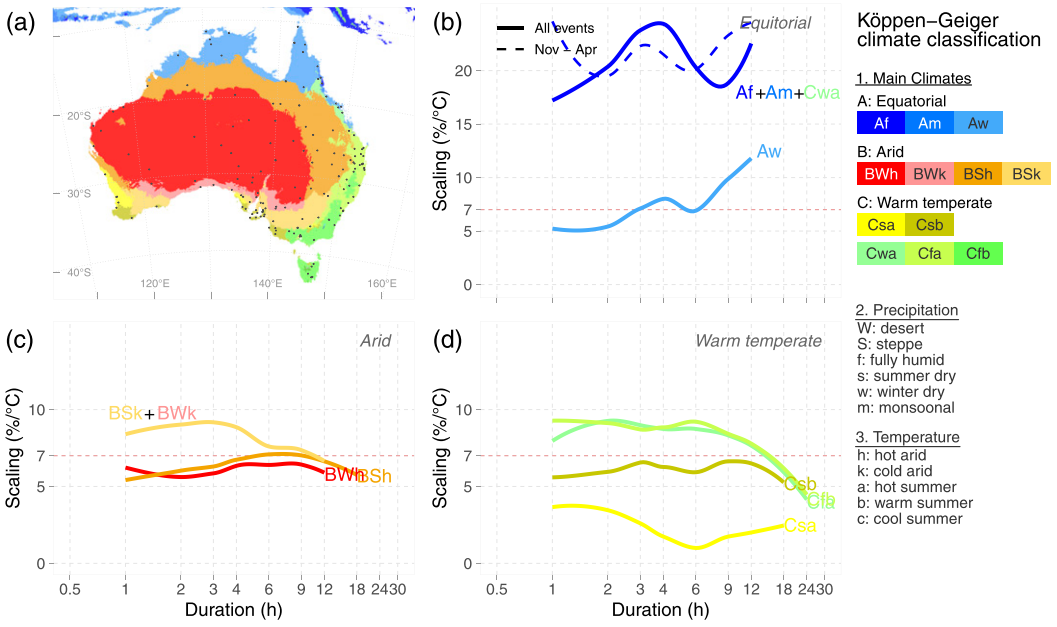

FIG. A2. As in Fig. 9, but for dewpoint temperature.

d. *Seasonal characteristics of precipitation–temperature relationships*

We find that strong seasonal variation in a location's temperature distribution and associated precipitation totals can produce very high scaling, exceeding seasonal-based results. Regions categorized by low-rainfall winter and high-rainfall summer seasons, such as Australia's tropical northeast coastline, require additional scrutinization over potential seasonal influences on scaling results such as the transition in dominant precipitation mechanism and associated precipitation totals. Seasonal differentiation is therefore recommended for regions with multiple distinct rainfall seasons or where the inclusion of a transitional period, such as a dry to wet month, has significant influence on scaling results. Subsetting on the basis of storm type might provide advantages over seasonal subsetting in the assessment of apparent scaling of distinct precipitation mechanisms, but is considerably more complex, requiring additional data to differentiate between convective and stratiform events such as cloud observations (Berg and Haerter 2013) or the presence of lightning (Molnar et al. 2015). It should be noted that lower-frequency variability (related to El Niño–Southern Oscillation or the interdecadal Pacific oscillation) (Pui et al. 2011 2012) can have a similar impact to the seasonal differentiation noted above, especially for regions where significant power is attributed to such anomalies.

e. *The use of daily data in apparent scaling analyses*

The use of daily precipitation totals in apparent scaling analyses should be avoided. Decreasing daily precipitation totals at higher temperatures due to the decreasing wet-time fraction, results in the development of strong hooks structures. Conditioning on wet-time fraction partially addresses this shortcoming; however, subdaily precipitation data are required, which presents the opportunity for the use of event-based methods, which are preferred as they explicability account for event attributes, such as duration, while allowing for temperature to be sampled prior to the start of the event to minimize the cooling effect of precipitation. Pairing of daily precipitation totals with mean daily temperatures over the same accumulation periods, risks a sampled temperature not being representative of the atmospheric state associated with the precipitation extreme (Visser et al. 2020).

f. *Concluding remarks*

The incorporation of event duration into apparent scaling analyses improves the robustness of apparent scaling results across temporal and spatial scales. Additionally, it allows for greater differentiation between potential impacts on different flood mechanisms; for example, flash flood events resulting from high to extremely high precipitation rates over short durations, and fluvial floods associated with precipitation events over longer durations. Assessing potential changes in flooding through changes in its key drivers, such as precipitation, is promoted over attempts to detect and extend historical flooding trends (Villarini and Wasko 2021). We find increasing extreme precipitation intensities with temperature across all event durations and climate zones analyzed, with higher apparent scaling rates for shorter-duration precipitation. Our results suggest an increase in precipitation intensities in line with historical trends and climate model predictions.

Acknowledgments. Conrad Wasko receives funding from the University of Melbourne McKenzie Postdoctoral Fellowships Program and Australian Research Council (ARC) Project DE210100479. This research was supported by the ARC Discovery Project DP200101326, and by industry support from Hydro Tasmania, Melbourne Water, Murray-Darling Basin

Authority, Queensland Department of Natural Resources Mines and Energy, Seqwater, Snowy Hydro, Sunwater, West Australian Water Corporation, and WaterNSW.

Data availability statement. Data were obtained from the Australian Bureau of Meteorology and can be found online (at http://www.bom.gov.au/climate/data/stations/).

APPENDIX

Dewpoint Temperature Apparent Scaling

Figures A1 and A2 are reproductions of Figs. 8 and 9 using dewpoint temperature instead of dry-bulb temperature as the temperature-scaling variable.

REFERENCES

Ali, H., and V. Mishra, 2017: Contrasting response of rainfall extremes to increase in surface air and dewpoint temperatures at urban locations in India. *Sci. Rep.*, **7**, 1228, https://doi.org/10.1038/s41598-017-01306-1.

——, H. J. Fowler, and V. Mishra, 2018: Global observational evidence of strong linkage between dew point temperature and precipitation extremes. *Geophys. Res. Lett.*, **45**, 12 320–12 330, https://doi.org/10.1029/2018GL080557.

——, ——, G. Lenderink, E. Lewis, and D. Pritchard, 2021: Consistent large-scale response of hourly extreme precipitation to temperature variation over land. *Geophys. Res. Lett.*, **48**, e2020GL090317, https://doi.org/10.1029/2020GL090317.

Allan, R. P., and B. J. Soden, 2008: Atmospheric warming and the amplification of precipitation extremes. *Science*, **321**, 1481–1484, https://doi.org/10.1126/science.1160787.

Bao, J., S. C. Sherwood, L. V. Alexander, and J. P. Evans, 2017: Future increases in extreme precipitation exceed observed scaling rates. *Nat. Climate Change*, **7**, 128–132, https://doi.org/10.1038/nclimate3201.

Barbero, R., S. Westra, G. Lenderink, and H. J. Fowler, 2018: Temperature-extreme precipitation scaling: A two-way causality? *Int. J. Climatol.*, **38**, e1274–e1279, https://doi.org/10.1002/joc.5370.

Beck, H. E., N. E. Zimmermann, T. R. McVicar, N. Vergopolan, A. Berg, and E. F. Wood, 2018: Present and future Köppen-Geiger climate classification maps at 1-km resolution. *Sci. Data*, **5**, 180214, https://doi.org/10.1038/sdata.2018.214.

Berg, P., and J. O. Haerter, 2013: Unexpected increase in precipitation intensity with temperature—A result of mixing of precipitation types? *Atmos. Res.*, **119**, 56–61, https://doi.org/10.1016/j.atmosres.2011.05.012.

——, ——, P. Thejll, C. Piani, S. Hagemann, and J. H. Christensen, 2009: Seasonal characteristics of the relationship between daily precipitation intensity and surface temperature. *J. Geophys. Res.*, **114**, D18102, https://doi.org/10.1029/2009JD012008.

——, C. Moseley, and J. O. Haerter, 2013: Strong increase in convective precipitation in response to higher temperatures. *Nat. Geosci.*, **6**, 181–185, https://doi.org/10.1038/ngeo1731.

Bui, A., F. Johnson, and C. Wasko, 2019: The relationship of atmospheric air temperature and dew point temperature to extreme rainfall. *Environ. Res. Lett.*, **14**, 074025, https://doi.org/10.1088/1748-9326/ab2a26.

Drobinski, P., B. Alonzo, S. Bastin, N. D. Silva, and C. Muller, 2016: Scaling of precipitation extremes with temperature in the French Mediterranean region: What explains the hook shape? *J. Geophys. Res. Atmos.*, **121**, 3100–3119, https://doi.org/10.1002/2015JD023497.

Emori, S., and S. J. Brown, 2005: Dynamic and thermodynamic changes in mean and extreme precipitation under changed climate. *Geophys. Res. Lett.*, **32**, L17706, https://doi.org/10.1029/2005GL023272.

Fowler, H. J., C. Wasko, and A. F. Prein, 2021a: Intensification of short-duration rainfall extremes and implications for flood risk: Current state of the art and future directions. *Philos. Trans. Roy. Soc.*, **379A**, 20190541, https://doi.org/10.1098/rsta.2019.0541.

——, and Coauthors, 2021b: Anthropogenic intensification of short-duration rainfall extremes. *Nat. Rev. Earth Environ.*, **2**, 107–122, https://doi.org/10.1038/s43017-020-00128-6.

Gaál, L., P. Molnar, and J. Szolgay, 2014: Selection of intense rainfall events based on intensity thresholds and lightning data in Switzerland. *Hydrol. Earth Syst. Sci.*, **18**, 1561–1573, https://doi.org/10.5194/hess-18-1561-2014.

Golroudbary, V. R., Y. Zeng, C. M. Mannaerts, and Z. Su, 2019: Response of extreme precipitation to urbanization over the Netherlands. *J. Appl. Meteor. Climatol.*, **58**, 645–661, https://doi.org/10.1175/JAMC-D-18-0180.1.

Haerter, J. O., P. Berg, and S. Hagemann, 2010: Heavy rain intensity distributions on varying time scales and at different temperatures. *J. Geophys. Res.*, **115**, D17102, https://doi.org/10.1029/2009JD013384.

Hardwick Jones, R., S. Westra, and A. Sharma, 2010: Observed relationships between extreme sub-daily precipitation, surface temperature, and relative humidity. *Geophys. Res. Lett.*, **37**, L22805, https://doi.org/10.1029/2010GL045081.

Held, I. M., and B. J. Soden, 2006: Robust responses of the hydrological cycle to global warming. *J. Climate*, **19**, 5686–5699, https://doi.org/10.1175/JCLI3990.1.

Kharin, V. V., F. W. Zwiers, X. Zhang, and G. C. Hegerl, 2007: Changes in temperature and precipitation extremes in the IPCC ensemble of global coupled model simulations. *J. Climate*, **20**, 1419–1444, https://doi.org/10.1175/JCLI4066.1.

Kim, S., S. Eghdamirad, A. Sharma, and J. H. Kim, 2020: Quantification of uncertainty in projections of extreme daily precipitation. *Earth Space Sci.*, **7**, e2019EA001052, https://doi.org/10.1029/2019EA001052.

Koenker, R., 2018: quantreg: Quantile regression, version 5.75. R Package, https://www.r-project.org.

——, and G. Bassett, 1978: Regression quantiles. *Econometrica*, **46**, 33–50, https://doi.org/10.2307/1913643.

Lenderink, G., and E. van Meijgaard, 2008: Increase in hourly precipitation extremes beyond expectations from temperature changes. *Nat. Geosci.*, **1**, 511–514, https://doi.org/10.1038/ngeo262.

——, and J. Attema, 2015: A simple scaling approach to produce climate scenarios of local precipitation extremes for the Netherlands. *Environ. Res. Lett.*, **10**, 085001, https://doi.org/10.1088/1748-9326/10/8/085001.

——, H. Y. Mok, T. C. Lee, and G. J. van Oldenborgh, 2011: Scaling and trends of hourly precipitation extremes in two different climate zones—Hong Kong and the Netherlands. *Hydrol. Earth Syst. Sci.*, **15**, 3033–3041, https://doi.org/10.5194/hess-15-3033-2011.

——, R. Barbero, S. Westra, and H. J. Fowler, 2018: Reply to comments on "Temperature-extreme precipitation scaling: A two-way causality?" *Int. J. Climatol.*, **38**, 4664–4666, https://doi.org/10.1002/joc.5799.

——, H. de Vries, H. J. Fowler, R. Barbero, B. van Ulft, and E. van Meijgaard, 2021: Scaling and responses of extreme

hourly precipitation in three climate experiments with a convection-permitting model. *Philos. Trans. Roy. Soc.*, **379A**, 20190544, https://doi.org/10.1098/rsta.2019.0544.

Loriaux, J. M., G. Lenderink, S. R. De Roode, and A. P. Siebesma, 2013: Understanding convective extreme precipitation scaling using observations and an entraining plume model. *J. Atmos. Sci.*, **70**, 3641–3655, https://doi.org/10.1175/JAS-D-12-0317.1.

Maeda, E. E., N. Utsumi, and T. Oki, 2012: Decreasing precipitation extremes at higher temperatures in tropical regions. *Nat. Hazards*, **64**, 935–941, https://doi.org/10.1007/s11069-012-0222-5.

Mauritsen, T., and B. Stevens, 2015: Missing iris effect as a possible cause of muted hydrological change and high climate sensitivity in models. *Nat. Geosci.*, **8**, 346–351, https://doi.org/10.1038/ngeo2414.

Molnar, P., S. Fatichi, L. Gaál, J. Szolgay, and P. Burlando, 2015: Storm type effects on super Clausius–Clapeyron scaling of intense rainstorm properties with air temperature. *Hydrol. Earth Syst. Sci.*, **19**, 1753–1766, https://doi.org/10.5194/hess-19-1753-2015.

O'Gorman, P. A., and C. J. Muller, 2010: How closely do changes in surface and column water vapor follow Clausius–Clapeyron scaling in climate change simulations? *Environ. Res. Lett.*, **5**, 025207, https://doi.org/10.1088/1748-9326/5/2/025207.

Panthou, G., A. Mailhot, E. Laurence, and G. Talbot, 2014: Relationship between surface temperature and extreme rainfalls: A multi-time-scale and event-based analysis. *J. Hydrometeor.*, **15**, 1999–2011, https://doi.org/10.1175/JHM-D-14-0020.1.

Park, I.-H., and S.-K. Min, 2017: Role of convective precipitation in the relationship between subdaily extreme precipitation and temperature. *J. Climate*, **30**, 9527–9537, https://doi.org/10.1175/JCLI-D-17-0075.1.

Peel, M. C., B. L. Finlayson, and T. A. Mcmahon, 2007: Updated world map of the Köppen-Geiger climate classification. *Hydrol. Earth Syst. Sci.*, **11**, 1633–1644, https://doi.org/10.5194/hess-11-1633-2007.

Peleg, N., F. Marra, S. Fatichi, P. Molnar, E. Morin, A. Sharma, and P. Burlando, 2018: Intensification of convective rain cells at warmer temperatures observed from high-resolution weather radar data. *J. Hydrometeor.*, **19**, 715–726, https://doi.org/10.1175/JHM-D-17-0158.1.

Pui, A., A. Lal, and A. Sharma, 2011: How does the Interdecadal Pacific Oscillation affect design floods in Australia? *Water Resour. Res.*, **47**, W05554, https://doi.org/10.1029/2010WR009420.

——, A. Sharma, A. Santoso, and S. Westra, 2012: Impact of the El Niño–Southern Oscillation, Indian Ocean dipole, and southern annular mode on daily to subdaily rainfall characteristics in east Australia. *Mon. Wea. Rev.*, **140**, 1665–1682, https://doi.org/10.1175/MWR-D-11-00238.1.

Roderick, T. P., C. Wasko, and A. Sharma, 2020: An improved covariate for projecting future rainfall extremes? *Water Resour. Res.*, **56**, e2019WR026924, https://doi.org/10.1029/2019WR026924.

Schleiss, M., 2018: How intermittency affects the rate at which rainfall extremes respond to changes in temperature. *Earth Syst. Dyn.*, **9**, 955–968, https://doi.org/10.5194/esd-9-955-2018.

Schroeer, K., and G. Kirchengast, 2017: Sensitivity of extreme precipitation to temperature: The variability of scaling factors from a regional to local perspective. *Climate Dyn.*, **50**, 3981–3994, https://doi.org/10.1007/s00382-017-3857-9.

Sugiyama, M., H. Shiogama, and S. Emori, 2010: Precipitation extreme changes exceeding moisture content increases in MIROC and IPCC climate models. *Proc. Natl. Acad. Sci. USA*, **107**, 571–575, https://doi.org/10.1073/pnas.0903186107.

Sun, Q., F. Zwiers, X. Zhang, and G. Li, 2020: A comparison of intra-annual and long-term trend scaling of extreme precipitation with temperature in a large-ensemble regional climate simulation. *J. Climate*, **33**, 9233–9245, https://doi.org/10.1175/JCLI-D-19-0920.1.

Trenberth, K. E., A. Dai, R. M. Rasmussen, and D. B. Parsons, 2003: The changing character of precipitation. *Bull. Amer. Meteor. Soc.*, **84**, 1205–1218, https://doi.org/10.1175/BAMS-84-9-1205.

Utsumi, N., S. Seto, S. Kanae, E. E. Maeda, and T. Oki, 2011: Does higher surface temperature intensify extreme precipitation? *Geophys. Res. Lett.*, **38**, L16708, https://doi.org/10.1029/2011GL048426.

Villarini, G., and C. Wasko, 2021: Humans, climate and streamflow. *Nat. Climate Change*, **11**, 725–726, https://doi.org/10.1038/s41558-021-01137-z.

Visser, J. B., C. Wasko, A. Sharma, and R. Nathan, 2020: Resolving inconsistencies in extreme precipitation-temperature sensitivities. *Geophys. Res. Lett.*, **47**, e2020GL089723, https://doi.org/10.1029/2020GL089723.

Wang, G., D. Wang, K. E. Trenberth, A. Erfanian, M. Yu, and G. Michael, 2017: The peak structure and future changes of the relationships between extreme precipitation and temperature. *Nat. Climate Change*, **7**, 268–274, https://doi.org/10.1038/nclimate3239.

Wasko, C., and A. Sharma, 2014: Quantile regression for investigating scaling of extreme precipitation with temperature. *Water Resour. Res.*, **50**, 3608–3614, https://doi.org/10.1002/2013WR015194.

——, and ——, 2015: Steeper temporal distribution of rain intensity at higher temperatures within Australian storms. *Nat. Geosci.*, **8**, 527–529, https://doi.org/10.1038/ngeo2456.

——, and R. Nathan, 2019: The local dependency of precipitation on historical changes in temperature. *Climatic Change*, **156**, 105–120, https://doi.org/10.1007/s10584-019-02523-5.

——, A. Sharma, and F. Johnson, 2015: Does storm duration modulate the extreme precipitation-temperature scaling relationship? *Geophys. Res. Lett.*, **42**, 8783–8790, https://doi.org/10.1002/2015GL066274.

——, R. M. Parinussa, and A. Sharma, 2016: A quasi-global assessment of changes in remotely sensed rainfall extremes with temperature. *Geophys. Res. Lett.*, **43**, 12 659–12 668, https://doi.org/10.1002/2016GL071354.

——, W. T. Lu, and R. Mehrotra, 2018: Relationship of extreme precipitation, dry-bulb temperature, and dew point temperature across Australia. *Environ. Res. Lett.*, **13**, 074031, https://doi.org/10.1088/1748-9326/aad135.

Westra, S., L. V. Alexander, and F. W. Zwiers, 2013: Global increasing trends in annual maximum daily precipitation. *J. Climate*, **26**, 3904–3918, https://doi.org/10.1175/JCLI-D-12-00502.1.

——, and Coauthors, 2014: Future changes to the intensity and frequency of short-duration extreme rainfall. *Rev. Geophys.*, **52**, 522–555, https://doi.org/10.1002/2014RG000464.

Xiao, C., P. Wu, L. Zhang, and L. Song, 2016: Robust increase in extreme summer rainfall intensity during the past four decades observed in China. *Sci. Rep.*, **6**, 38506, https://doi.org/10.1038/srep38506.

Yin, J., S. Guo, P. Gentine, S. C. Sullivan, L. Gu, S. He, J. Chen, and P. Liu, 2021: Does the hook structure constrain future flood intensification under anthropogenic climate warming? *Water Resour. Res.*, **57**, e2020WR028491, https://doi.org/10.1029/2020WR028491.

Zhang, W., G. Villarini, and M. Wehner, 2019: Contrasting the responses of extreme precipitation to changes in surface air and dew point temperatures. *Climatic Change*, **154**, 257–271, https://doi.org/10.1007/s10584-019-02415-8.

Zhang, X., F. W. Zwiers, G. Li, H. Wan, and A. J. Cannon, 2017: Complexity in estimating past and future extreme short-duration rainfall. *Nat. Geosci.*, **10**, 255–259, https://doi.org/10.1038/ngeo2911.